Received: 13 May 2018 | Revised: 27 October 2018 | Accepted: 26 November 2018

DOI: 10.1002/hipo.23064

WILEY

RAPID COMMUNICATION

Recurrent connections between CA2 pyramidal cells

Kazuki Okamoto[1] | **Yuji Ikegaya**[1,2]

[1]Laboratory of Chemical Pharmacology, Graduate School of Pharmaceutical Sciences, The University of Tokyo, Tokyo, Japan

[2]Center for Information and Neural Networks, National Institute of Information and Communications Technology, Suita, Japan

Correspondence
Yuji Ikegaya, Laboratory of Chemical Pharmacology, Graduate School of Pharmaceutical Sciences, The University of Tokyo, 7-3-1 Hongo, Bunkyo-ku, Tokyo 113-0033, Japan.
Email: yuji@ikegaya.jp

Funding information
International Research Center for Neurointelligence (WPI-IRCN); Human Frontier Science Program, Grant/Award Number: RGP0019/2016; Grants-in-Aid for Scientific Research, Grant/Award Numbers: 17K19441, 18H05114

Abstract

Recurrent excitatory synapses have theoretically been shown to play roles in memory storage and associative learning and are well described to occur in the CA3 region of the hippocampus. Here, we report that the CA2 region also contains recurrent excitatory monosynaptic couplings. Using dual whole-cell patch-clamp recordings from CA2 pyramidal cells in mouse hippocampal slices under differential interference contrast microscopic controls, we evaluated monosynaptic excitatory connections. Unitary excitatory postsynaptic potentials occurred in 1.4% of 502 cell pairs. These connected pairs were preferentially located in the superficial layer and proximal part (CA2b) of the CA2 region. These results indicate that recurrent excitatory circuits are denser in the CA2 region than in the CA1 region, as well as in the CA3 region.

KEYWORDS

hippocampus, CA2, monosynapse, connectivity

1 | INTRODUCTION

Theoretical studies have suggested that reentrant positive-feedback excitation of the neuronal network is critical for nonlinear information processing, including memory storage, associative learning, and pattern separation/completion (Amari, Cichocki, & Yang, 1996; Hebb, 1949; Hopfield, 1982; Kohonen, 1998). The hippocampal CA3 region is one of the candidate brain regions that anatomically contain self-associative excitatory networks and functionally exert this information processing (Guzman, Schlogl, Frotscher, & Jonas, 2016; MacVicar & Dudek, 1981; Miles & Wong, 1986; Nakazawa, McHugh, Wilson, & Tonegawa, 2004; Treves & Rolls, 1994). However, few studies have directly measured monosynaptic recurrent connections in the hippocampus (Deuchars & Thomson, 1996; Guzman et al., 2016; Miles & Wong, 1986), particularly in the CA2 region (Mercer, Eastlake, Trigg, & Thomson, 2012).

The CA2 region of the hippocampus is unique in terms of spatial representation and social memory (Hitti & Siegelbaum, 2014; Mankin, Diehl, Sparks, Leutgeb, & Leutgeb, 2015); however, it has been less investigated because it is not included in the classical tri-synaptic pathway and the CA2 region is anatomically small, which limits experimental access. Notably, whether CA2 pyramidal cells are mutually excited at the monosynaptic level remains controversial, although several reports suggest that the CA2 region contains recurrent excitatory circuits (Lu, Igarashi, Witter, Moser, & Moser, 2015) partly because CA2 neurons can initiate sharp wave/ripple (SWR) oscillations (Oliva, Fernandez-Ruiz, Buzsaki, & Berenyi, 2016).

In the present study, we directly measured excitatory monosynaptic connections between CA2 pyramidal cells using double whole-cell patch-clamp recordings. We observed monosynaptic unitary excitatory postsynaptic potentials (EPSPs) between 1.4% of the CA2 pyramidal cell pairs. The CA2-to-CA2 connections existed preferentially in the CA2b subarea and exhibited a preferential spatial direction.

2 | RESULTS AND DISCUSSION

Recent histological studies have broadened the conventional definition (Lorente de Nó, 1934) of the CA2 region based on specific molecular expressions, such as those of G-protein signaling protein 14 (RGS14) and striatal-enriched protein tyrosine phosphatase (STEP; Dudek, Alexander, & Farris, 2016; Kohara et al., 2014; Lein, Callaway, Albright, & Gage, 2005; Noguchi, Matsumoto, Morikawa, Tamura, & Ikegaya, 2017). We also confirmed that RGS14 immunoreactivity indicated the macroscopic location of the CA2 region in transverse slices of the hippocampus. The vast majority (94.8%) of RGS14-positive cells

were also immunopositive against STEP (Supporting Information S1). However, at the single cell level, RGS14-positive cells were sparse near the CA1/CA2 and CA2/CA3 borders (Figure 1). This sparsity was particularly prevalent in the ventral hippocampus. Thus, the salt-and-pepper distribution of RGS14-positive cells indicates that a significant number of non-CA2 pyramidal cells (presumably CA1 or CA3 pyramidal cells) are present in the CA2 region. A small number of RGS14-positive cells were likely to be located even beyond the region borders and existed in the CA1 and CA3 regions.

We investigated recurrent CA2 connectivity by recording unitary EPSPs between two CA2 pyramidal cells. We visually targeted pyramidal cells using a differential interference contrast microscope. The recorded neurons were intracellularly filled with biocytin through patch-clamp pipettes and were subsequently immunostained using an antibody against RGS14 or STEP (Figure 2a). A train of four action potentials was evoked at 20 Hz in one of the recorded cells, and the evoked membrane potentials were monitored for the other cells (Figure 2b). In the 502 pairs tested, we found seven chemical synaptic connections and no electrical coupling; that is, the CA2-to-CA2 synaptic connection probability was 1.4%. There was no correlation between the postnatal ages of the mice and the connectivity of the CA2 pyramidal cells (Supporting Information S2). The unitary EPSPs had a mean peak amplitude of 0.43 ± 0.14 mV and a mean transmission failure rate of 54 ± 24% (mean ± standard deviation [SD] of seven connections). The mean resting membrane potentials of the postsynaptic CA2 cells and the other nonpaired CA2 cells were − 55 ± 12 mV (n = 7 cells) and − 60.4 ± 5.6 mV, respectively (n = 14 cells; p = .19, t_{19} = 1.4, Student's t test). Three of the seven connections exhibited short-term depression in response to four presynaptic spikes (Figure 3a,b; Pair #1: $p = 3.5 \times 10^{-3}$ between first and third EPSP, $p = 5.2 \times 10^{-4}$ between first and fourth EPSP, Pair #2: $p = 2.4 \times 10^{-4}$ between first and third EPSP, $p = 5.2 \times 10^{-3}$ between first and fourth EPSP, Pair #3: p = .04 between first and third EPSP, $p = 1.8 \times 10^{-4}$ between first and fourth EPSP, p = .03 between second and fourth EPSP, n = 50 trials each, Wilcoxon signed-rank test with Bonferroni correction after Friedman test). The other four pairs did not exhibit short-term plasticity (Supporting Information S3A; p > .05, Friedman test). The histograms of the EPSP amplitudes indicate that the distributions had multiples peaks, which suggest that CA2-CA2 synapses are connected through one or a few release sites (Figure 3c and Supporting Information S3B); however, we did not conduct quantum analyses because of insufficient numbers of the data. Incidentally, we targeted adjacent cell pairs and occasionally observed capacitive couplings, which were typically identified as waveforms time-locked with presynaptic action potentials (Figure 3a, bottom), consistent with previous studies using multiple patch-clamp recordings (Couey et al., 2013; Guzman et al., 2016). In these cases, we distinguished the postsynaptic response from capacitive coupling by referring to the latencies from the presynaptic spike peaks.

We also patched 108 CA3 pyramidal cell pairs and found three chemical synaptic connections (2.8%), whose unitary EPSPs had a mean peak amplitude of 0.75 ± 0.54 mV and a mean failure rate of 45 ± 22% (three connections; Supporting Information S4). These CA3 pyramidal cell pairs were recorded mainly from the CA3a,b subarea with optical targeting. For CA3a cells, CA3 pyramidal cells were post hoc determined based on their RGS14-negativity. The parameters of the CA3 pairs are similar to those reported in previous studies of CA3 connections (Guzman et al., 2016; Miles & Wong, 1986).

We failed to identify characteristic differences in the EPSP amplitudes and failure rates between the CA2-CA2 and CA3-CA3 pairs (Student's t test); however, this might be due to insufficient data for the CA3 pairs. We found short-term depression in one CA3 pair (Supporting Information S3; Pair #3: $p = 2.1 \times 10^{-3}$ between 1st and 2nd EPSP, $p = 6.2 \times 10^{-6}$ between first and third EPSP, $p = 2.5 \times 10^{-5}$ between first and fourth EPSP, p = .03 between second and third EPSP, n = 50 trials each, Wilcoxon signed-rank test with Bonferroni correction after Friedman test). The CA3-CA3 transmission is reported to exhibit short-term depression for 20-Hz trains at room

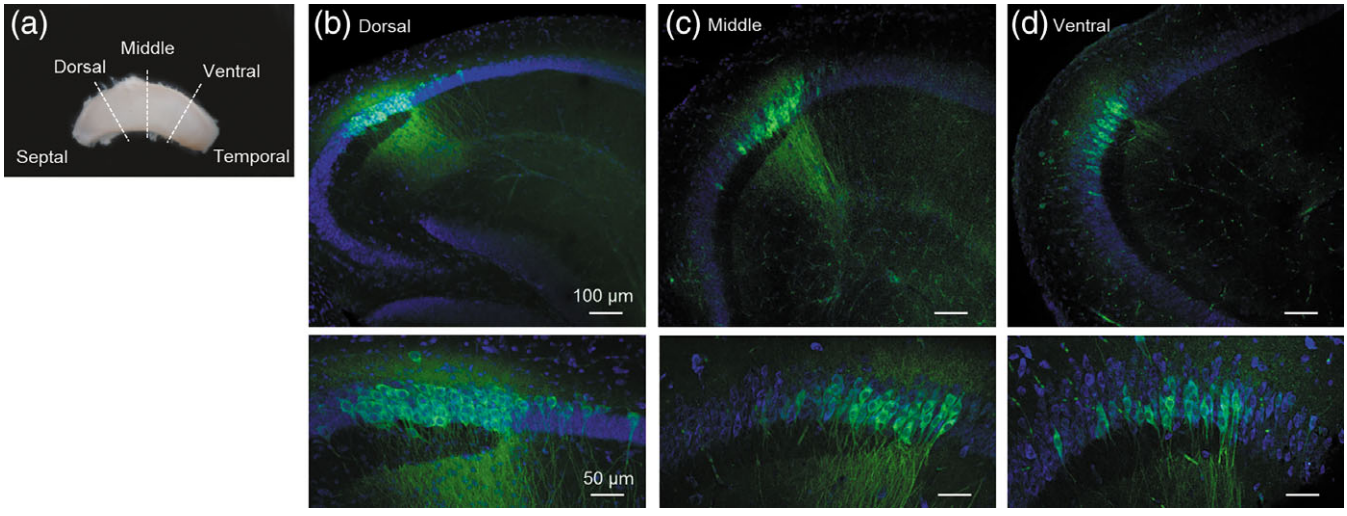

FIGURE 1 Distributions of CA2 pyramidal cells along the longitudinal axis of the mouse hippocampus. (a) A whole hippocampus was transversely sectioned at the dorsal, middle, and ventral areas, indicated by the broken white lines. (b–d) The transverse sections at the dorsal (b), middle (c), and ventral (d) areas were labeled with an anti-RGS14 antibody (*green*, a CA2 marker) and NeuroTrace 435/455 Nissl stain (*blue*). The bottom photos are magnified images of the CA2 region, indicating that the CA2 borders next to the CA1 and CA3 regions are ambiguous because of the sparse distribution of the CA2 pyramidal cells, particularly in the ventral hippocampus [Color figure can be viewed at wileyonlinelibrary.com]

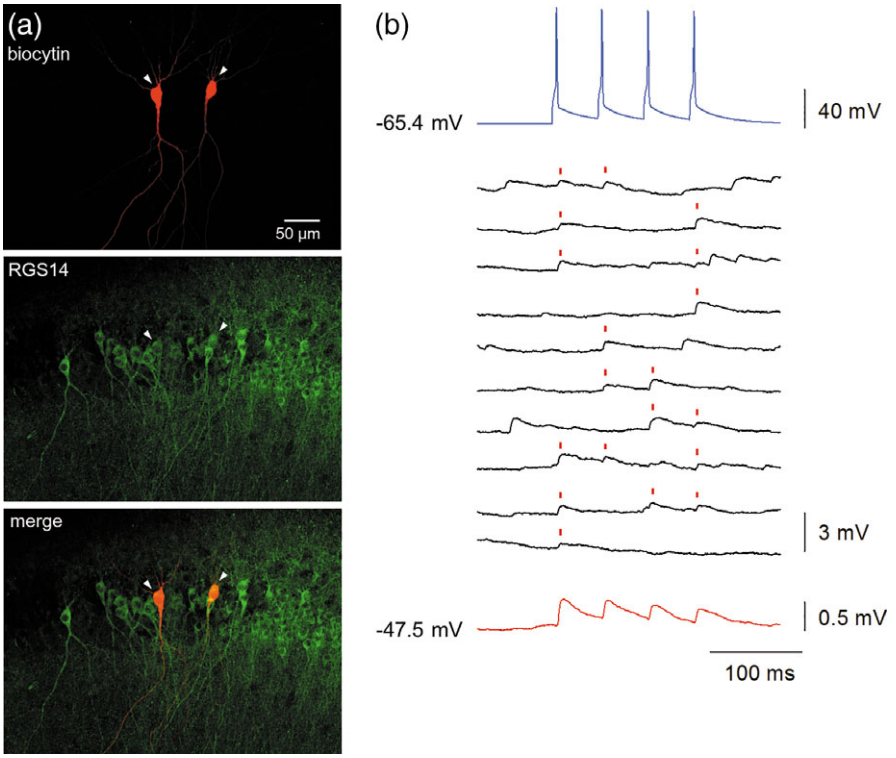

FIGURE 2 Monosynaptic recurrent connection of a CA2-CA2 pair. (a) *Top*: Confocal images of a synaptically connected pair of CA2 pyramidal cells that were filled with biocytin (*red*). *Middle*: The CA2 region was immunostained for RGS14 (*green*). *Bottom*: RGS14 was expressed in the recorded cells. (b) Unitary EPSPs of the connected pair. *Top*: Mean trace of a train of current injection-induced action potentials of the presynaptic cell (blue, averaged for 50 traces). *Middle*: Representative postsynaptic membrane responses recorded in the current-clamp mode for the successive trials (black). *Bottom*: An average of 50 recorded traces for the postsynaptic cell [Color figure can be viewed at wileyonlinelibrary.com]

temperature, with moderate facilitation at 34°C (Guzman et al., 2016). In contrast, CA1-CA1 connections exhibit short-term depression at 34–36°C (Deuchars & Thomson, 1996). Short-term plasticity is also dependent on the extracellular ionic solution. Our experimental conditions, in which the $[Mg^{2+}]/[Ca^{2+}]$ radio was 0.54, are thought to evoke strong initial releases of glutamate during spike trains (Debanne, Guerineau, Gahwiler, & Thompson, 1996). For the CA2-CA2 connections, we found that at 32–34°C, three synaptic pairs were short-term depressive, in contrast to the other four pairs (Figure 3 and Supporting Information S3). We found that the first EPSP amplitudes were not correlated with the paired-pulse ratios (R = 0.50, p = .49, n = 7 pairs, least-square linear regression). Thus, we concluded that CA2-CA2 pairs are heterogeneous in short-term plasticity.

The mean transmission latency in the CA2 pairs, the 10–90% rise time, and the decay time constant were 3.7 ± 1.2 ms, 3.8 ± 1.0 ms, and 17.0 ± 4.4 ms, respectively (Supporting Information S5B). The mean transmission latency in the CA3 pairs, the 10–90% rise time, and the decay time constant were 4.4 ± 1.5 ms, 4.7 ± 1.7 ms, and 42.7 ± 5.1 ms, respectively. The decay time constant in the CA2 pairs was significantly shorter than that in the CA3 pairs (Supporting Information S5, n = 3–7 pairs; $p = 3.9 \times 10^{-5}$, t_8 = 8.1, Student's t test), while neither the mean latency nor the rise time differed between CA2 and CA3 pairs (n = 3–7 pairs; latency: p = .42, t_8 = 0.85; 10–90% rise time: t_8 = 1.1, p = .31, Student's t test). These results were consistent with a report that indicated the half width of an EPSP slope in CA2 pairs was shorter than that of CA1 pairs (Mercer et al., 2012), which suggests that CA2 pyramidal cells receive temporally short EPSPs. The decay time constant depends on the recording temperature (Deuchars & Thomson, 1996; Guzman et al., 2016), as well as the distance from the soma to the input site (Magee & Cook, 2000). We did not histologically confirm the exact location of the synaptic contacts between CA2 pairs; however, we recorded EPSPs at 32–34°C. Thus, it is possible that the decay time constants in our data may be shorter than those recorded at room temperature in these previous reports; however, it should be noted that we identified a difference in the time decay between CA2 and CA3 pairs under identical conditions.

During the whole-cell recordings, we measured the physical distances between the somata of two recorded cells in the images obtained with a differential interference contrast microscope. The intersoma distances were not correlated with the connection probability (Figure 4). This result appears to be similar to the previously reported spatial patterns of CA3 connectivity (Guzman et al., 2016); however, it is different from those of neocortical connectivity, in which more adjacent pairs had a higher probability of connections (Peng, Barreda Tomas, Klisch, Vida, & Geiger, 2017; Perin, Berger, & Markram, 2011; Song, Sjostrom, Reigl, Nelson, & Chklovskii, 2005). When considering the connectivity, however, the anatomical size of the CA2 region must be considered; the majority of CA2 cell pairs have intersoma distances of less than 100 μm. Thus, we cannot rule out the possibility that this sampling restriction masked the distance dependence.

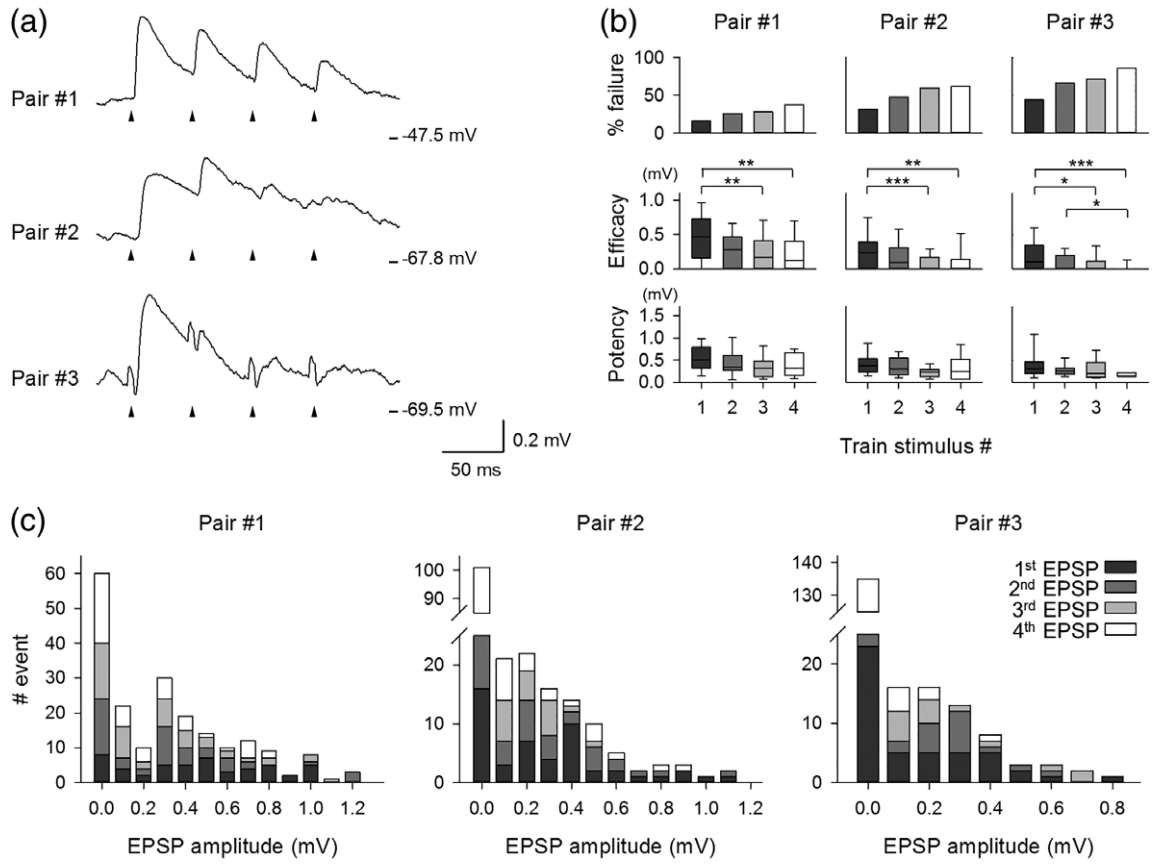

FIGURE 3 Unitary EPSP properties of CA2-CA2 connected pairs. (a) Three examples of the averaged traces of postsynaptic responses following presynaptic spike trains (four pulses at 20 Hz) in all 50 stimulus trials in synaptically connected CA2 pairs. Arrowheads indicate presynaptic spike peak points. The trace of pair #3 contained capacitive coupling, which was time-locked to presynaptic action potentials. (b) *Top:* The percentages of synaptic failures in response to a presynaptic spike train (four pulses at 20 Hz) for three connected pairs. Train stimuli were repeated 50 times. *Center:* Synaptic efficacies across the 50 trains (including failure events). $^{*}p < .05$, $^{**}p < .01$, $^{***}p < .001$, $n = 50$ trains each, Wilcoxon signed-rank test with Bonferroni correction after Friedman test. *Bottom:* Synaptic potencies (without failure events). (c) Histograms of the EPSP peak amplitudes for three connected CA2 pairs

CA1 and CA3 pyramidal cells are heterogeneous along both transverse (Ishizuka, Weber, & Amaral, 1990; Lee, Wang, Deshmukh, & Knierim, 2015; Lu et al., 2015; Sun et al., 2017) and radial axes (Kohara et al., 2014; Lee et al., 2014; Valero et al., 2015). Similar heterogeneity has also been reported in the CA2 region (Oliva et al., 2016). We thus investigated whether CA2-to-CA2 connections are spatially biased in the CA2 stratum pyramidale. For one of the seven connections, we failed to accurately identify the relative loci of the recorded cells in the RGS14-positive CA2 region. Thus, we analyzed the remaining 6 pairs. The relative location of each recorded cell was determined in the CA2 stratum pyramidale, which was deformed into a virtual rectangular coordinate. The transverse axis was replotted so that zero corresponded to the end tip of the stratum lucidum, whereas zero in the radial axis was set to correspond to the midpoint in the thickness of the stratum pyramidale (Figure 5a,b). In this cell map, we identified two structural tendencies. First, the directions from presynaptic cells to postsynaptic cells were spatially biased (Figure 5c; $V = 2.3$, $p = .01$, $n = 6$ pairs, V-test). A given CA2 pyramidal cell tended to make a synaptic connection with a CA2 pyramidal cell that was more proximal to the CA3 regions. This tendency suggests that compared to distal CA2 cells, more proximal CA2 pyramidal cells receive more recurrent inputs from other CA2 pyramidal cells.

Second, the connected pairs were located preferentially in the superficial layer and the proximal side of the CA2 region (Figure 5d). The difference between the superficial and deep layers of the stratum pyramidale has not been adequately investigated in the CA2 region. A recent study demonstrated that CA2 neurons are capable of initiating SWR oscillations and that SWR-preceding activity is different in the superficial and deep sublayers in the CA2 region (Oliva et al., 2016). Because recurrent excitation is believed to trigger SWRs (Traub, Miles, & Wong, 1989), our results are consistent with SWR generation in the CA2 region; however, Oliva et al. (2016) reported that CA2 cells in the deep layer were activated earlier than CA2 cells in the superficial layer during SWR. In contrast, our results indicate that the recurrent connections of the CA2 pyramidal cells are nearly exclusively located in the superficial layer. Moreover, active cells are reported to exist more abundantly in the CA2 superficial layer, and they are more likely to activate interneurons. This process may be involved in the generation of SWR. The SWR generation is thought to be a complex process, including dense recurrent circuits, timed interneuron activation (Stark et al., 2014), and extrahippocampal controls (Buzsaki, 2015). Therefore, the CA2 region may trigger SWR independent of local recurrent excitation.

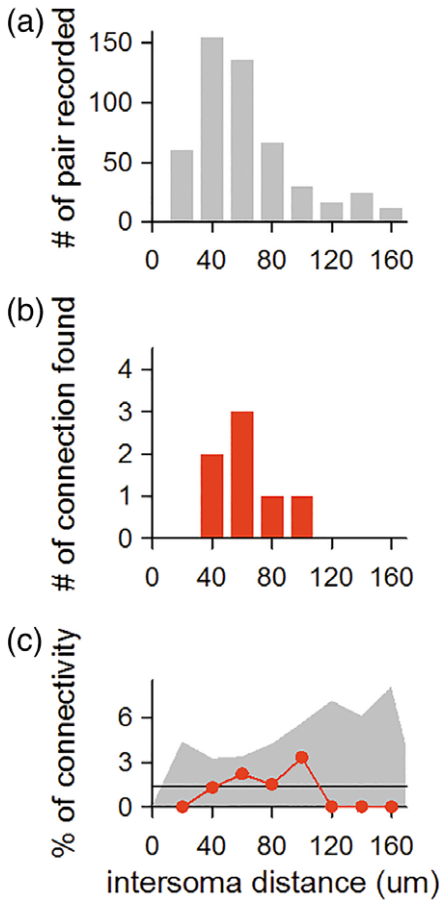

FIGURE 4 Lack of correlation of CA2-CA2 connections with their intercell distances. (a) The histogram indicates the distributions of the distances between the centroids of the cell bodies of all recorded pairs. (b) The histogram indicates the same distribution as the top, but for only the synaptically connected pairs. (c) The graph plots the connection probabilities (i.e., the histogram in (b) divided by the histogram in (a)) as a function of the intersoma distance (red). The black line is the mean connection probability (1.4%). The gray area is the 95% confidence interval estimated by 10,000 randomly resampled surrogates [Color figure can be viewed at wileyonlinelibrary.com]

We found that the proximal CA2 (CA2b) subarea, but not the distal CA2 (CA2a) subarea, has dense recurrent connections, similar to the CA3 region. According to the most recent definition (Dudek et al., 2016; Lein et al., 2005), the CA2b subarea encompasses the stratum lucidum and receives monosynaptic inputs from the dentate gyrus (Kohara et al., 2014; Sun et al., 2017); however, the unitary EPSP sizes are smaller in CA2 pyramidal cells than in CA3 pyramidal cells (Sun et al., 2017). In addition, CA2 pyramidal cells receive strong excitatory inputs in the stratum lacunosum-moleculare from the entorhinal cortex (Chevaleyre & Siegelbaum, 2010). These extrahippocampal inputs contribute to the unstable dynamics of CA2 neuronal activity (Lee et al., 2015; Lu et al., 2015; Mankin et al., 2015). The CA3 network contains clustered circuit motifs (Guzman et al., 2016). The neocortex also contains rich clustered connections (Peng et al., 2017; Perin et al., 2011; Song et al., 2005). In CA2 pyramidal cells, we did not identify bidirectionally connected pairs, which may be because the numbers of pair recordings are not sufficient.

A previous study reported a very low connection probability (0.22%) between CA2 pyramidal cells (Mercer et al., 2012); however, this study did not identify CA2 pyramidal cells histologically using CA2 cell markers (RGS14 or STEP). Given that CA2 pyramidal cells are sparse even in the CA2 pyramidal cell layer, the authors may have underestimated the true CA2 connectivity. Another possibility is that they might have focused more on the CA2a subarea, which was conventionally defined as "the CA2 region". This sampling bias could also lead to an underestimation of the CA2 connectivity.

The CA2 region has been reported to contain a higher density of GABAergic interneurons than the CA1 or CA3 region (Leranth & Ribak, 1991; Mercer, Trigg, & Thomson, 2007). CA2 pyramidal cells receive strong inhibitory inputs (Sun et al., 2017). Inhibitory interneurons are often activated by spike transmission; that is, an action potential of a single excitatory cell can induce a postsynaptic discharge of fast-spiking interneurons (Jouhanneau, Kremkow, & Poulet, 2018), as well as a transient oscillation (Bazelot, Telenczuk, & Miles, 2016). However, we did not observe di-synaptic inhibition in postsynaptic CA2 cells following presynaptic CA2 cells, which may be because our recording conditions were not optimized to record inhibitory synaptic inputs. If this is the case, potentially occurring, but undetected GABAergic input may mask EPSPs, leading to an underestimation of the connectivity ratio (currently 1.4%) of CA2 pairs. However, this possibility does not affect our main conclusion that recurrent excitatory connections exist between CA2 pyramidal cells. We also consider another possibility that a single action potential of a CA2 pyramidal cell is not sufficiently strong to fire postsynaptic interneurons in our slice preparations. We encountered two cases of excitatory connections from a CA2 pyramidal cell to a fast-spiking interneuron in the CA2 stratum pyramidale. Their mean EPSP amplitudes were 0.77 and 0.89 mV, which were too small to evoke an action potential in the postsynaptic cells.

Interestingly, within the CA3 region, the CA3a subarea receives more inhibitory inputs and has denser recurrent connectivity than the CA3b subarea (Sun et al., 2017). These observations suggest similar circuit properties of the CA2b and CA3a subareas. The high density of recurrent excitatory connections may be counterbalanced by strong inhibitory inputs and maintain the excitatory-to-inhibitory balance in the CA2 local circuit.

3 | METHODS

3.1 | Animal experiment ethics

Experiments were performed with the approval of the Animal Experiment Ethics Committee at the University of Tokyo (approval no. P29-9) and according to the University of Tokyo guidelines for the care and use of laboratory animals. Institute of Cancer Research (ICR) mice (SLC) were housed in cages under standard laboratory conditions (12 hr light/dark cycle, ad libitum access to food and water). All efforts were made to minimize the animals' suffering and the number of animals used.

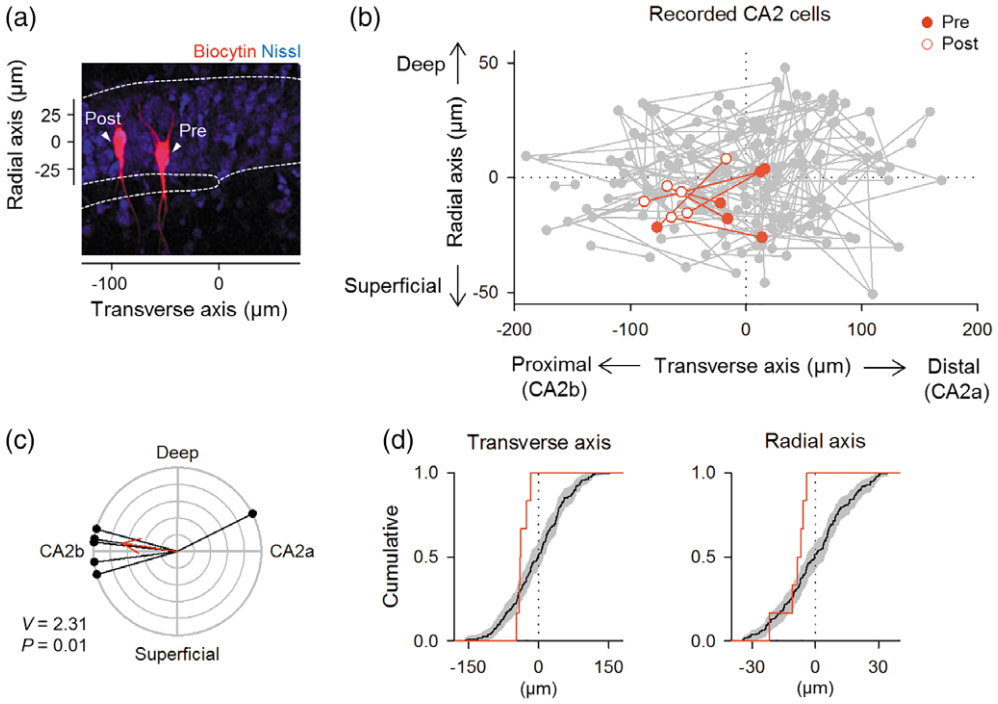

FIGURE 5 Spatial bias of CA2-CA2 connections. (a) A confocal image of a synaptically connected pair of CA2 pyramidal cells that were filled with biocytin (*red*). The stratum pyramidale and the end of the stratum lucidum were determined using fluorescent Nissl staining (*blue*). (b) Cell map for all recorded pairs of CA2 pyramidal cells. Gray dots and lines indicate the soma location of the CA2 pyramidal cells and their potential connections (unconnected), respectively. Red lines represent the synaptic connections ($n = 6$). Red filled and open circles indicate the soma location of the presynaptic and postsynaptic cells, respectively. The transverse axis indicates the position relative to the end tip of the stratum lucidum. As to the radial axis, the midpoint in the thickness of the stratum pyramidale was defined as zero. (c) A polar plot of the intersoma directions of the synaptically connected pairs. Each black line indicates the direction from the soma of one presynaptic cell to the soma of its postsynaptic cell. The red arrow represents the mean vector of all six connected pairs. $V = 2.3$, $p = .01$, V test. (d) Cumulative distributions of the midpoints between two soma locations of connected pairs (*red line*) and unconnected pairs (*black line*) along the transverse axis (*left*) and the radial axis (*right*). The gray areas indicate the 95% confidence intervals estimated by Kaplan–Meier method [Color figure can be viewed at wileyonlinelibrary.com]

3.2 | Acute slice preparation

Acute slices were prepared from the hippocampi of ICR mice (17–28 postnatal days). The mice were anesthetized with isoflurane and subsequently decapitated. The brains were removed and placed in an ice-cold oxygenated solution that consisted of (in mM) 222.1 sucrose, 27 $NaHCO_3$, 1.4 NaH_2PO_4, 2.5 KCl, 1 $CaCl_2$, 7 $MgSO_4$, and 0.5 ascorbic acid. The brains were sliced horizontally at a thickness of 400 μm using a VT1200S vibratome (Leica). The slices, including the middle part in the longitudinal axis of the hippocampus, were allowed to equilibrate at room temperature for at least 0.5 hr while submerged in a chamber filled with oxygenated aCSF that consisted of (in mM) 127 NaCl, 26 $NaHCO_3$, 1.6 KCl, 1.24 KH_2PO_4, 1.3 $MgSO_4$, 2.4 $CaCl_2$, and 10 glucose. The slices were mounted in a recording chamber and perfused at a rate of 1.5–3 ml/min with oxygenated aCSF.

3.3 | In vitro electrophysiology

All recordings were performed at 32–34°C. Whole-cell recordings were collected from up to four CA2 pyramidal cells using a MultiClamp 700B amplifier and a Digidata 1550 digitizer controlled by pCLAMP10.6 software (Molecular Devices). Borosilicate glass pipettes (3–6 MΩ) were filled with a solution that contained (in mM) 135 K-gluconate, 4 KCl_2, 0.3 EGTA, 10 HEPES, 10 Na_2-phosphocreatine, 4 Mg ATP, 0.3 Na_2 GTP, and 2.0 biocytin. The signals were gained 10-fold, low-pass filtered at 1 kHz and digitized at 20 kHz. The existence of synaptic connectivity was assessed by averaging 50 successive traces in which four spikes at 20 Hz were induced by current injection in presynaptic cells.

3.4 | Analysis

Unitary EPSPs were mainly analyzed using Clampfit software (Molecular Devices). Paired responses were considered successful when the EPSP slopes exceeded a threshold of 3 × *SD*s of the preceding voltage fluctuations. The latency of an EPSP was measured as the time interval between the presynaptic action potential peak and the onset of the postsynaptic EPSP rise. The rise time was measured as the time interval between the points of 10% and 90% of the peak amplitude. To measure the decay time constant, we fit a mono-exponential function to the trace between the first EPSP peak and the second EPSP onset.

3.5 | Histology

CA2 pyramidal cells were intracellularly perfused with 2 mM biocytin for whole-cell recordings. After the recordings, the slices were fixed for at least 20 hr at 4°C in 0.1 M Na_3PO_4, pH 7.4, which contained

3% (w/v) formaldehyde. The sections were incubated with 2 μg/ml streptavidin-Alexa Fluor 594 conjugate and 0.2% Triton X-100 for 6 hr, followed by incubation with 0.4% NeuroTrace 435/455 blue-fluorescent Nissl Stain (Thermo Fisher Scientific; N21479) overnight. The tissue sections were subsequently incubated with mouse primary antibodies for RGS14 (NeuroMab; N133/21; 1:500) or STEP (Cell Signaling Technology; 4396S; 1:500) for 16 hr at 4°C, followed by incubation with a secondary goat antibody to mouse IgG (Thermo Fisher Scientific; A-11001; 1:500) for 6 hr at 4°C. For the double immunostaining in Supporting Information S1, we used a rabbit primary anti-RGS14 antibody (Sigma; SPA046847; 1:500).

ACKNOWLEDGMENTS

We thank Dr. Segundo Jose Guzman, Dr. Vivien Chevaleyre, Dr. Rebecca Piskorowski, and Dr. Takeshi Sakaba for their comments on the experiment. This work was supported by Grants-in-Aid for Scientific Research (17K19441 and 18H05114) and the Human Frontier Science Program (RGP0019/2016). This work was conducted, in part, as a program at the International Research Center for Neurointelligence (WPI-IRCN) of the University of Tokyo Institutes for Advanced Study at the University of Tokyo.

ORCID

Yuji Ikegaya https://orcid.org/0000-0003-2260-8191

REFERENCES

Amari S, Cichocki A, Yang HH. 1996. A new learning algorithm for blind signal separation. In Advances in Neural Information Processing Systems. (pp. 757–763).

Bazelot, M., Telenczuk, M. T., & Miles, R. (2016). Single CA3 pyramidal cells trigger sharp waves in vitro by exciting interneurones. *The Journal of Physiology*, *594*(10), 2565–2577.

Buzsaki, G. (2015). Hippocampal sharp wave-ripple: A cognitive biomarker for episodic memory and planning. *Hippocampus*, *25*(10), 1073–1188.

Chevaleyre, V., & Siegelbaum, S. A. (2010). Strong CA2 pyramidal neuron synapses define a powerful disynaptic cortico-hippocampal loop. *Neuron*, *66*(4), 560–572.

Couey, J. J., Witoelar, A., Zhang, S. J., Zheng, K., Ye, J., Dunn, B., … Witter, M. P. (2013). Recurrent inhibitory circuitry as a mechanism for grid formation. *Nature Neuroscience*, *16*(3), 318–324.

Debanne, D., Guerineau, N. C., Gahwiler, B. H., & Thompson, S. M. (1996). Paired-pulse facilitation and depression at unitary synapses in rat hippocampus: Quantal fluctuation affects subsequent release. *The Journal of Physiology*, *491*(Pt 1), 163–176.

Deuchars, J., & Thomson, A. M. (1996). CA1 pyramid-pyramid connections in rat hippocampus in vitro: Dual intracellular recordings with biocytin filling. *Neuroscience*, *74*(4), 1009–1018.

Dudek, S. M., Alexander, G. M., & Farris, S. (2016). Rediscovering area CA2: Unique properties and functions. *Nature Reviews Neuroscience*, *17*(2), 89–102.

Guzman, S. J., Schlogl, A., Frotscher, M., & Jonas, P. (2016). Synaptic mechanisms of pattern completion in the hippocampal CA3 network. *Science*, *353*(6304), 1117–1123.

Hebb, D. O. (1949). *The organization of behavior; a neuropsychological theory*. New York: Wiley xix, 335 p. p.

Hitti, F. L., & Siegelbaum, S. A. (2014). The hippocampal CA2 region is essential for social memory. *Nature*, *508*(7494), 88–92.

Hopfield, J. J. (1982). Neural networks and physical systems with emergent collective computational abilities. *Proceedings of the National Academy of Sciences of the United States of America*, *79*(8), 2554–2558.

Ishizuka, N., Weber, J., & Amaral, D. G. (1990). Organization of intrahippocampal projections originating from CA3 pyramidal cells in the rat. *The Journal of Comparative Neurology*, *295*(4), 580–623.

Jouhanneau, J. S., Kremkow, J., & Poulet, J. F. A. (2018). Single synaptic inputs drive high-precision action potentials in parvalbumin expressing GABA-ergic cortical neurons in vivo. *Nature Communications*, *9*(1), 1540.

Kohara, K., Pignatelli, M., Rivest, A. J., Jung, H. Y., Kitamura, T., Suh, J., et al. (2014). Cell type-specific genetic and optogenetic tools reveal hippocampal CA2 circuits. *Nature Neuroscience*, *17*(2), 269–279.

Kohonen, T. (1998). The self-organizing map. *Neurocomputing*, *21*, 1–6.

Lee, H., Wang, C., Deshmukh, S. S., & Knierim, J. J. (2015). Neural population evidence of functional heterogeneity along the CA3 transverse axis: Pattern completion versus pattern separation. *Neuron*, *87*(5), 1093–1105.

Lee, S. H., Marchionni, I., Bezaire, M., Varga, C., Danielson, N., Lovett-Barron, M., … Soltesz, I. (2014). Parvalbumin-positive basket cells differentiate among hippocampal pyramidal cells. *Neuron*, *82*(5), 1129–1144.

Lein, E. S., Callaway, E. M., Albright, T. D., & Gage, F. H. (2005). Redefining the boundaries of the hippocampal CA2 subfield in the mouse using gene expression and 3-dimensional reconstruction. *The Journal of Comparative Neurology*, *485*(1), 1–10.

Leranth, C., & Ribak, C. E. (1991). Calcium-binding proteins are concentrated in the CA2 field of the monkey hippocampus: A possible key to this region's resistance to epileptic damage. *Experimental Brain Research*, *85*(1), 129–136.

Lorente De Nó, R. (1934). Studies of the structure of the cerebral cortex. II. Continuation of the study of the ammonic system. *Journal für Psychologie und Neurologie*, *46*, 113–177.

Lu, L., Igarashi, K. M., Witter, M. P., Moser, E. I., & Moser, M. B. (2015). Topography of place maps along the CA3-to-CA2 axis of the hippocampus. *Neuron*, *87*(5), 1078–1092.

MacVicar, B. A., & Dudek, F. E. (1981). Electrotonic coupling between pyramidal cells: A direct demonstration in rat hippocampal slices. *Science*, *213*(4509), 782–785.

Magee, J. C., & Cook, E. P. (2000). Somatic EPSP amplitude is independent of synapse location in hippocampal pyramidal neurons. *Nature Neuroscience*, *3*(9), 895–903.

Mankin, E. A., Diehl, G. W., Sparks, F. T., Leutgeb, S., & Leutgeb, J. K. (2015). Hippocampal CA2 activity patterns change over time to a larger extent than between spatial contexts. *Neuron*, *85*(1), 190–201.

Mercer, A., Eastlake, K., Trigg, H. L., & Thomson, A. M. (2012). Local circuitry involving parvalbumin-positive basket cells in the CA2 region of the hippocampus. *Hippocampus*, *22*(1), 43–56.

Mercer, A., Trigg, H. L., & Thomson, A. M. (2007). Characterization of neurons in the CA2 subfield of the adult rat hippocampus. *The Journal of Neuroscience*, *27*(27), 7329–7338.

Miles, R., & Wong, R. K. (1986). Excitatory synaptic interactions between CA3 neurones in the guinea-pig hippocampus. *The Journal of Physiology*, *373*, 397–418.

Nakazawa, K., McHugh, T. J., Wilson, M. A., & Tonegawa, S. (2004). NMDA receptors, place cells and hippocampal spatial memory. *Nature Reviews Neuroscience*, *5*(5), 361–372.

Noguchi, A., Matsumoto, N., Morikawa, S., Tamura, H., & Ikegaya, Y. (2017). Juvenile hippocampal CA2 region expresses aggrecan. *Frontiers in Neuroanatomy*, *11*, 41.

Oliva, A., Fernandez-Ruiz, A., Buzsaki, G., & Berenyi, A. (2016). Role of hippocampal CA2 region in triggering sharp-wave ripples. *Neuron*, *91*(6), 1342–1355.

Peng, Y., Barreda Tomas, F. J., Klisch, C., Vida, I., & Geiger, J. R. P. (2017). Layer-specific organization of local excitatory and inhibitory synaptic connectivity in the rat presubiculum. *Cerebral Cortex*, *27*(4), 2435–2452.

Perin, R., Berger, T. K., & Markram, H. (2011). A synaptic organizing principle for cortical neuronal groups. *Proceedings of the National Academy of Sciences of the United States of America*, *108*(13), 5419–5424.

Song, S., Sjostrom, P. J., Reigl, M., Nelson, S., & Chklovskii, D. B. (2005). Highly nonrandom features of synaptic connectivity in local cortical circuits. *PLoS Biology*, *3*(3), e68.

Stark, E., Roux, L., Eichler, R., Senzai, Y., Royer, S., & Buzsaki, G. (2014). Pyramidal cell-interneuron interactions underlie hippocampal ripple oscillations. *Neuron*, *83*(2), 467–480.

Sun, Q., Sotayo, A., Cazzulino, A. S., Snyder, A. M., Denny, C. A., & Siegelbaum, S. A. (2017). Proximodistal heterogeneity of hippocampal CA3 pyramidal neuron intrinsic properties, connectivity, and reactivation during memory recall. *Neuron*, *95*(3), 656–672 e3.

Traub, R. D., Miles, R., & Wong, R. K. (1989). Model of the origin of rhythmic population oscillations in the hippocampal slice. *Science*, *243*(4896), 1319–1325.

Treves, A., & Rolls, E. T. (1994). Computational analysis of the role of the hippocampus in memory. *Hippocampus*, *4*(3), 374–391.

Valero, M., Cid, E., Averkin, R. G., Aguilar, J., Sanchez-Aguilera, A., Viney, T. J., … de la Prida, L. M. (2015). Determinants of different deep and superficial CA1 pyramidal cell dynamics during sharp-wave ripples. *Nature Neuroscience*, *18*(9), 1281–1290.

SUPPORTING INFORMATION

Additional supporting information may be found online in the Supporting Information section at the end of the article.

How to cite this article: Okamoto K, Ikegaya Y. Recurrent connections between CA2 pyramidal cells. *Hippocampus*. 2018;1–8. https://doi.org/10.1002/hipo.23064